bioRxiv preprint doi: https://doi.org/10.1101/2020.10.09.333195; this version posted October 12, 2020. The copyright holder for this preprint (which was not certified by peer review) is the author/funder. All rights reserved. No reuse allowed without permission.

Mathematical formulation and application of kernel tensor decomposition based unsupervised feature extraction

Y-h. Taguchi[a,*], Turki Turki[b]

[a]Department of Physics, Chuo University, Tokyo 112-8551, Japan
[b]Department of Computer Science, King Abdulaziz University, Jeddah, 21589, Saudi Arabia

ABSTRACT

In this work, we extended the recently developed tensor decomposition (TD) based unsupervised feature extraction (FE) to a kernel based method, through a mathematical formulation. Subsequently, the kernel TD (KTD) based unsupervised FE was applied to two synthetic examples as well as real data sets, and the relevant findings were compared with those obtained previously using the TD based unsupervised FE approaches. The KTD based unsupervised FE demonstrated the most competitive performance against the TD based unsupervised FE in *large p small n* situations, involving a limited number of samples with many variables (observations). Nevertheless, the KTD based unsupervised FE outperformed the TD based unsupervised FE in non *large p small n* situations. In general, although the use of the kernel trick can help the TD based unsupervised FE gain more variations, a wider range of problems may also be encountered. Considering the comparable performance of the KTD based unsupervised FE and TD based unsupervised FE when applied to *large p small n* problems, it is expected that the KTD based unsupervised FE can be applied in the genomic science domain, which involves many *large p small n* problems, and in which, the TD based unsupervised FE approach has been effectively applied.

Introduction

Recently, the tensor decomposition (TD) and principal component analysis (PCA) based unsupervised feature extraction (FE) (Taguchi, 2020) approach was developed to identify a limited number of genes in *large p small n* problems involving a small number of samples (n) with a large number of features (genes) (p). This approach, applied to genomic science applications, which frequently involve *large p small n* problems, could successfully identify the limited number of biologically reliable genes that cannot be selected using conventional statistical test based feature selection methods. Nevertheless, because the TD and PCA based unsupervised FE do not include any tunable parameters owing to their linearity, the methods cannot be modified or optimized in failure scenarios. Thus, it is desirable to extend the TD and PCA based unsupervised FE to include non-linearity.

To this end, we aimed at extending the TD based unsupervised FE to incorporate the kernel trick (Schölkopf, 2000) to introduce non-linearity. Because tensors do not have inner products that can be replaced with non-linear kernels, we incorporate the self-inner products of tensors. In particular, the inner product is replaced with non-linear kernels, and TD is applied to the generated tensor including non-linear kernels. In this framework, the TD can be easily "kernelized".

Several researchers have attempted to apply kernel methods to process tensor data. For instance, Signoretto et al. (2011); Signoretto et al. (2012) and Zhao et al. (2013b,a)) input tensors into vectors (or matrices), which were then used to construct the kernels. However, such conversion may destroy the structural information of the tensor data. Moreover, the dimensionality of the resulting vector is typically extremely high, which leads to the curse of dimensionality and small sample size problems (Liu et al. (2015), Yan et al. (2007)). He et al. (2017) proposed an implementation in which the tensor was reproduced using a kernelized TD.

It is expected that these problems can be avoided by computing the inner product of the tensors, as realized in the proposed approach.

*Corresponding author
tag@granular.com (Y-h. Taguchi)
ORCID(s): 0000-0003-0867-8986 (Y-h. Taguchi); 0000-0002-9491-2435 (T. Turki)

bioRxiv preprint doi: https://doi.org/10.1101/2020.10.09.333195; this version posted October 12, 2020. The copyright holder for this preprint (which was not certified by peer review) is the author/funder. All rights reserved. No reuse allowed without permission.

Results

Mathematical formulations

Suppose there exists a tensor $x_{ijk} \in \mathbb{R}^{N\times M\times K}$, which represents the value of the ith feature of the samples with properties j and k. For example, x_{ijk} might represent the price of product i that a person with a gender k and age j previously bought. In this case, N is the number of products available, M is the age, and $K \in [1, 2]$ represents male or female. Alternatively, in genomic science applications, which is the focus domain of this work, x_{ijk} is the expression of the ith genes of the kth tissue of the jth person; in this case, N is the number of genes, M is the number of participants in the study, and K is the number of tissues for which the expression of genes is to be measured. As another example, x_{ijk} might represent the electric current of the ith circuit at the jth temperature and kth atomic pressure; in this case, N is the number of circuits in a machine, and M and K denote the number of recordings of the temperature and atomic pressure, respectively.

The aim of TD based unsupervised FE is to select the limited number of critical features among all the features (as many as N). In the first case, when i represents a product, the purpose of analysis may be to identify the limited number of products, the buyers of which are restricted to specific ages and genders. In the second case, when i represents a gene, the purpose of analysis may be to determine the limited number of genes whose altered expression may cause diseases. In the third example, when i is a circuit, the purpose of analysis may be to identify the limited number of circuits whose malfunctioning may result in the failure of the machine. Thus, in general, the purpose of TD based unsupervised FE is to screen a small part of the large features that are of significance.

In this regard, in TD based unsupervised FE, higher order singular value decomposition (Taguchi, 2020) (HOSVD) is applied to x_{ijk} to yield

$$x_{ijk} = \sum_{\ell_1=1}^{N}\sum_{\ell_2=1}^{M}\sum_{\ell_3=1}^{K} G(\ell_1\ell_2\ell_3)u_{\ell_1 i}u_{\ell_2 j}u_{\ell_3 k} \tag{1}$$

where $G(\ell_1\ell_2\ell_3) \in \mathbb{R}^{N\times M\times K}$ is a core tensor, which represents the weight of product $u_{\ell_1 i}u_{\ell_2 j}u_{\ell_3 k}$ of the contribution to x_{ijk}. $u_{\ell_1 i} \in \mathbb{R}^{N\times N}, u_{\ell_2 j} \in \mathbb{R}^{M\times M}, u_{\ell_3 k} \in \mathbb{R}^{K\times K}$ denote singular value vectors that represent the various dependencies of x_{ijk} on i, j, k, respectively; these vectors are orthogonal matrices.

To select the critical is, we must specify $u_{\ell_1 i}$ to select is; The is must be those for which the absolute values of $u_{\ell_1 i}$ are large. In this context, we must first identify $u_{\ell_2 j}$ and $u_{\ell_3 k}$, which represent the properties of interest. In the first example, the absolute value of $u_{\ell_2 j}$, which corresponds to the age, must be larger than a specific age. $u_{\ell_3 j}$, which corresponds to the genders, must be assigned distinct values for the two genders. In the second example, $u_{\ell_2 j}$, which corresponds to study participants, must be assigned distinct values for the patients and healthy controls. $u_{\ell_3 j}$, which corresponds to tissues, must have distinct values for the different tissues. In the third example, $u_{\ell_2 j}$ and $u_{\ell_3 k}$ must be assigned extremely large values at specific temperatures and atomic pressures.

After identifying the $u_{\ell_2 j}$ and $u_{\ell_3 k}$ of interest, we attempt to identify $G(\ell_1\ell_2\ell_3)$ that have larger absolute values given ℓ_2 and ℓ_3. Once ℓ_1 with G having the large absolute values is specified, we attempt to identify i with large absolute values of $u_{\ell_1 i}$. These is might represent the critical products bought by persons with specific ages and gender, genes expressive in certain specific tissues of patients, and circuits in which the electric current increases drastically at specific temperatures and atomic pressures.

The application of TD based unsupervised FE to problems in genomic science yielded satisfactory results even when conventional feature selection methods based upon statistical tests failed (Taguchi, 2020; Taguchi and Turki, 2020; Ng and Taguchi, 2020). Nevertheless, TD based unsupervised FE involve certain limitations. Specifically, owing to the tunable parameters, this approach cannot be modified or optimized in failure scenarios. The proposed method aims at extending the TD based unsupervised FE to be incorporated with kernel tricks (Schölkopf, 2000). In this scenario, because many kernels to be selected, a better strategy can likely be identified to be applied to the target problems.

To apply the kernel trick, TD must be suitably modified. First, we consider the partial sum as

$$x_{jkj'k'} = \sum_i x_{ijk}x_{ij'k'} \tag{2}$$

bioRxiv preprint doi: https://doi.org/10.1101/2020.10.09.333195; this version posted October 12, 2020. The copyright holder for this preprint (which was not certified by peer review) is the author/funder. All rights reserved. No reuse allowed without permission.

Substituting Eq. (1) into the aforementioned equation yields

$$x_{jkj'k'} = \sum_i \sum_{\ell_1=1}^{N} \sum_{\ell_2=1}^{M} \sum_{\ell_3=1}^{K} G(\ell_1\ell_2\ell_3) u_{\ell_1 i} u_{\ell_2 j} u_{\ell_3 k} \sum_{\ell'_1=1}^{N} \sum_{\ell'_2=1}^{M} \sum_{\ell'_3=1}^{K} G(\ell'_1\ell'_2\ell'_3) u_{\ell'_1 i} u_{\ell'_2 j'} u_{\ell'_3 k'} \tag{3}$$

$$= \sum_{\ell_1=1}^{N} \sum_{\ell_2=1}^{M} \sum_{\ell_3=1}^{K} \sum_{\ell'_1=1}^{N} \sum_{\ell'_2=1}^{M} \sum_{\ell'_3=1}^{K} G(\ell_1\ell_2\ell_3) u_{\ell_2 j} u_{\ell_3 k} G(\ell'_1\ell'_2\ell'_3) u_{\ell'_2 j'} u_{\ell'_3 k'} \sum_i u_{\ell_1 i} u_{\ell'_1 i} \tag{4}$$

$$= \sum_{\ell_1=1}^{N} \sum_{\ell_2=1}^{M} \sum_{\ell_3=1}^{K} \sum_{\ell'_1=1}^{N} \sum_{\ell'_2=1}^{M} \sum_{\ell'_3=1}^{K} G(\ell_1\ell_2\ell_3) u_{\ell_2 j} u_{\ell_3 k} G(\ell'_1\ell'_2\ell'_3) u_{\ell'_2 j'} u_{\ell'_3 k'} \delta_{\ell_1 \ell'_1} \tag{5}$$

$$= \sum_{\ell_2=1}^{M} \sum_{\ell_3=1}^{K} \sum_{\ell'_2=1}^{M} \sum_{\ell'_3=1}^{K} \left(\sum_{\ell_1=1}^{N} G(\ell_1\ell_2\ell_3) G(\ell_1\ell'_2\ell'_3) \right) u_{\ell_2 j} u_{\ell_3 k} u_{\ell'_2 j'} u_{\ell'_3 k'} \tag{6}$$

Thus, we can obtain $u_{\ell_2 j}$ and $u_{\ell_3 k}$ by applying the HOSVD to Eq. (2) as

$$x_{jkj'k'} = \sum_{\ell_2} \sum_{\ell_3} \sum_{\ell'_2} \sum_{\ell'_3} G(\ell_2\ell_3\ell'_2\ell'_3) u_{\ell_2 j} u_{\ell_3 k} u_{\ell'_2 j} u_{\ell'_3 k}. \tag{7}$$

Note that when using the linear kernel, as indicated in Eq. (2), the KTD is equivalent to the (linear) TD.

Because Eq. (2) is expressed in the form of an inner product, it can be easily extended to (non-linear) kernels. Although in the presented analysis, we only considered the radial base function (RBF) kernel as an example, any other kernel can be used in place of the RBF kernel. Eq. (2) can be easily extended to the RBF kernel as

$$x_{jkj'k'} = \exp\left\{ -\alpha \sum_i \left(x_{ijk} - x_{ij'k'} \right)^2 \right\} \tag{8}$$

to which the HOSVD can be applied as is. This operation generates an expression corresponding to Eq. (7) with distinct Gs and $u_{\ell_2 j}, u_{\ell_3 k}, u_{\ell'_2 j}, u_{\ell'_3 k}$s.

To integrate two matrices x_{ij} and x_{kj} that share the sample j, we consider

$$x_{jj'} = \sum_{j''} \sum_i x_{ij} x_{ij''} \sum_k x_{kj''} x_{kj'} \tag{9}$$

to which the singular value decomposition (SVD) can be applied as is

$$x_{jj'} = \sum_\ell u_{\ell j} \lambda_\ell v_{\ell j'} \tag{10}$$

This expression can be easily extended to the RBF kernel as

$$x_{jj'} = \sum_{j''} \left[\exp\left\{ -\alpha \sum_i \left(x_{ij} - x_{ij''} \right)^2 \right\} \exp\left\{ -\alpha' \sum_k \left(x_{kj''} - x_{kj'} \right)^2 \right\} \right] \tag{11}$$

to which the SVD can be applied as is, and an expression similar to Eq. (10) can be obtained with distinct $u_{\ell j}, \lambda_\ell, v_{\ell j'}$

Finally, if two matrices, x_{ij} and x_{ik}, share feature i, we have

$$x_{jk} = \sum_i x_{ij} x_{ik} \tag{12}$$

to which the SVD can be applied as is, yielding

$$x_{jk} = \sum_\ell u_{\ell j} \lambda_\ell v_{\ell k}. \tag{13}$$

bioRxiv preprint doi: https://doi.org/10.1101/2020.10.09.333195; this version posted October 12, 2020. The copyright holder for this preprint (which was not certified by peer review) is the author/funder. All rights reserved. No reuse allowed without permission.

This expression can be easily extended to the RBF kernel as

$$x_{jk} = \exp\left\{-\alpha \sum_i \left(x_{ij} - x_{ik}\right)^2\right\} \tag{14}$$

to which the SVD can be applied as is, and we can obtain an expression similar to Eq. (13) with distinct $u_{\ell j}, \lambda_\ell, v_{\ell k}$s.

Application to various data sets

The KTD based unsupervised FE was applied to various datasets (Fig. 1).

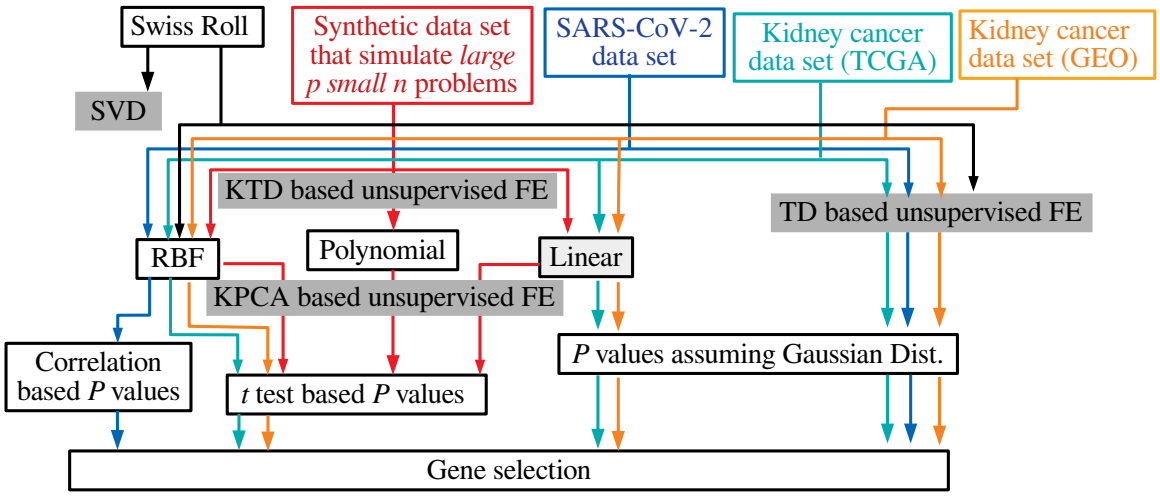

Figure 1: Overview of performed analyses

Swiss Roll

To verify if the TD extended to the kernel (KTD approach) can capture the non-linearity, the Swiss Roll framework is considered, represented as $x_{ijk} \in \mathbb{R}^{N\times 3\times 10}$

$$p_i = -1 + \frac{2i}{N}, 1 \leq i \leq N \tag{15}$$

$$x_{i1k} = p_i \cos\left(2\pi p_i\right) \tag{16}$$

$$x_{i2k} = -1 + \varepsilon_{ijk} \tag{17}$$

$$x_{i3k} = p_i \sin\left(2\pi p_i\right) \tag{18}$$

where ε_{ijk} is drawn the from uniform distribution between -1 and 1 (x_{ij1} is shown in Fig. 2(A)). Here, $\sum_j x_{ijk} = 0, \sum_i x_{ijk} = N, N = 1000$. This expression is equivalent to that of 10 ensembles of Swiss Rolls, each of which are generated with distinct ε_{ijk}. To verify that the linear method cannot capture non-linear structures (i.e., the order of i along the curved space) of the Swiss Roll, we apply the SVD to the x_{ij1} shown in Fig. 2(A). Figure 2(B) shows $u_{\ell i}, 1 \leq \ell \leq 3$. Clearly, the SVD cannot capture the non-lineer structure of the Swiss Roll. Moreover, even when the HOSVD is applied to x_{ijk}, the non-linear structure is not well captured (Fig. 2(C)). The kernel based tensor can be generated as

$$x_{iki'k'} = \exp\left\{-\alpha \sum_j \left(x_{ijk} - x_{i'jk'}\right)^2\right\}, \ \alpha = 10^{-2} \tag{19}$$

to which the HOSVD can be applied to yield

$$x_{iki'k'} = \sum_{\ell_1}\sum_{\ell_3}\sum_{\ell'_1}\sum_{\ell'_3} G(\ell_1\ell_3\ell'_1\ell'_3) u_{\ell_1 i} u_{\ell_3 k} u_{\ell'_1 i'} u_{\ell'_3 k'}. \tag{20}$$

bioRxiv preprint doi: https://doi.org/10.1101/2020.10.09.333195; this version posted October 12, 2020. The copyright holder for this preprint (which was not certified by peer review) is the author/funder. All rights reserved. No reuse allowed without permission.

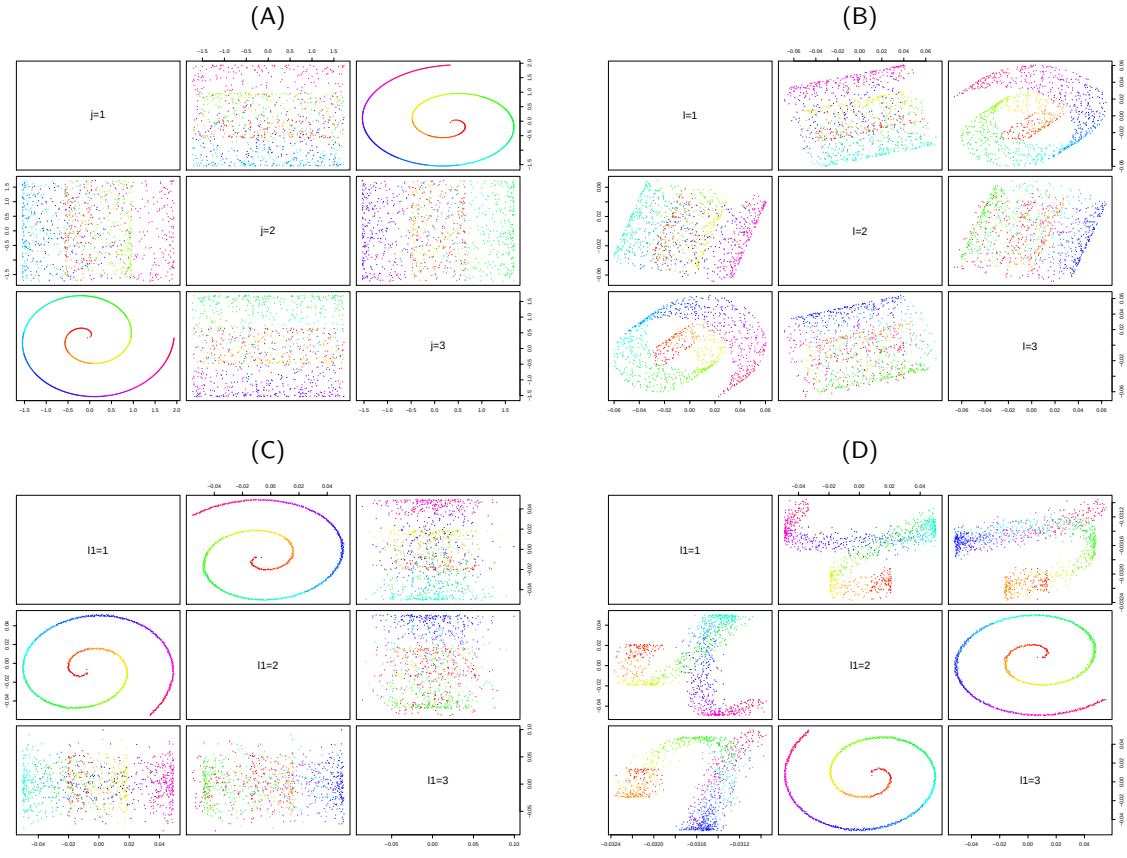

Figure 2: Swiss roll. The colors represent the direction of i (1 to N) in gradation. (A) x_{ij1}, (B) $u_{\ell i}, 1 \leq \ell \leq 3$ by SVD, (C) $u_{\ell_1 i}, 1 \leq \ell \leq 3$ by HOSVD, (D) $u_{\ell_1 i}, 1 \leq \ell \leq 3$ by kernel (RBF) based HOSVD.

$u_{\ell_1 i}, 1 \leq \ell_1 \leq 3$ represents the non-linear structure to a certain extent (Fig. 2(D)). Thus, by replacing the inner product of the tensor with kernels, the developed TD can identify the non-linear structure of the Swiss Roll, at least partially.

Although in the aforementioned synthetic example, the KTD based unsupervised FE can successfully identify the non-linear structure of Swiss Roll, which cannot be captured by the original (linear) TD based unsupervised FE, the key intent of the TD based unsupervised FE is to realize the feature selection in *large p small n* problems, with $p \gg n$. Thus, we must examine if the KTD based unsupervised FE can outperform the TD based unsupervised FE in *large p small n* problems.

Large p small n problem

We consider the following synthetic example: $x_{ijk} \in \mathbb{R}^{N \times M \times M}$, as

$$x_{ijk} \sim \begin{cases} \mathcal{N}(\mu, \sigma) & i \leq N_1 \leq N, j, k \leq \frac{M}{2} \\ \mathcal{N}(0, \sigma) & \text{otherwise} \end{cases} \tag{21}$$

where $\mathcal{N}(\mu, \sigma)$ is the Gaussian distribution of the mean μ and standard deviation σ. This problem is slightly challenging as it is a two class problem although it appears to be a four class problem. We apply the KTD as well as the kernel PCA (KPCA) as

$$K(x_{ijk}, x_{ij'k'}) = \sum_i x_{ijk} x_{ij'k'} \tag{22}$$

$$= \exp\left\{ -\alpha \sum_i \left(x_{ijk} - x_{ij'k'} \right)^2 \right\} \tag{23}$$

bioRxiv preprint doi: https://doi.org/10.1101/2020.10.09.333195; this version posted October 12, 2020. The copyright holder for this preprint (which was not certified by peer review) is the author/funder. All rights reserved. No reuse allowed without permission.

Table 1
Geometric mean P-values computed through the t tests performed on singular value vectors determined using the KTD and KPCA. Smaller P-values are better. $N = 1000, N_1 = 10, M = 6, \mu = 2, \sigma = 1$.

Kernel	RBF ($\alpha = 10^{-6}$)		RBF ($\alpha = 10^{-3}$)		linear	
P-values	raw	corrected	raw	corrected	raw	corrected
KTD	8.19×10^{-3}	4.31×10^{-2}	1.95×10^{-2}	9.22×10^{-2}	7.18×10^{-3}	3.87×10^{-2}
KPCA	9.45×10^{-3}	2.59×10^{-1}	1.45×10^{-2}	3.89×10^{-1}	7.30×10^{-3}	2.01×10^{-1}
Kernel	polynomial ($d = 2$)		polynomial ($d = 3$)			
P-values	raw	corrected	raw	corrected		
KTD	1.36×10^{-1}	4.38×10^{-1}	3.03×10^{-1}	3.61×10^{-1}		
KPCA	7.43×10^{-2}	6.43×10^{-1}	2.28×10^{-1}	3.81×10^{-1}		

$$= \left(1 + \sum_i x_{ijk} x_{ij'k'}\right)^d \tag{24}$$

The expressions correspond to the linear, RBF and polynomial kernels (from top to bottom). When the KPCA is applied, a tensor, x_{ijk}, is unfolded to a matrix, $x_{i(jk)} \in \mathbb{R}^{N \times M^2}$.

The performance evaluation is realized as follows. For the KTD, $u_{\ell j} u_{\ell k}, 1 \leq \ell \leq M$, are divided into two classes, $j, k \leq \frac{M}{2}$, or others, for each ℓ. A two way t test is performed on these classes. The computed M P-values for each ℓ are corrected considering the BH criterion (Taguchi, 2020), and the smallest P-value is recorded. This process is repeated one hundred times, while generating new random variables from the Gaussian distribution. The geometric mean of the P-value is computed as a performance measure. For the KPCA, $u_{\ell(jk)}, 1 \leq \ell \leq M^2$ are divided into two classes for each ℓ, and the computed M^2 P-values for each ℓ are corrected using BH criterion. The smallest P-value is recorded. This process is repeated one hundred times, while generating new random variables from the Gaussian distribution used to generate x_{ijk}. The geometric mean of the P-value is computed as a performance measure. Table 1 presents the results of this analysis. It can be noted that the raw P-values for the KPCA and KTD are not considerably different; nevertheless, the corrected P-values are smaller in the KTD than those for the RBF and linear kernel. In other words, the KTD can effectively identify the singular value vectors coincident in the two classes with a smaller number of singular value vectors. Nevertheless, the RBF could not outperform the linear kernel. We implemented other α values for the RBF kernel, but the RBF kernel could not outperform the linear kernel through any of the α values. This finding suggests that in *large p small n* situations, the introduction of non-linearity in the kernel is not entirely beneficial, which is likely why the TD based unsupervised FE could outperform the conventional statistical methods despite its linearity. Furthermore, the introduction of the non-linearity in the kernels could not not improve the performance in *large p small n* situations even when the KTD based unsupervised FE was applied to real problems, as described in the following sections.

We also examined if the restriction of $u_{\ell(jk)}$ to $1 \leq \ell \leq M$ could improve the performance of the KPCA owing to the smaller number of P-values considered in the results. Nevertheless, the performance was not performed, thereby indicating that the smallest P-values for the KPCA lies in $\ell > M$, and thus, $u_{\ell(jk)}, M < \ell \leq M^2$ cannot be neglected.

SARS-CoV-2 data set

We applied the KTD based unsupervised FE to real data sets. The first dataset corresponded to the repurposing of drugs for COVID-19, which the TD based unsupervised FE was successfully applied to the gene expression profiles of SARS-CoV-2 infected cell lines (Taguchi and Turki, 2020). In particular, the TD based unsupervised FE could predict many promising drugs including ivermectin, the clinical trials using which have been recently initiated. Herein, we briefly summarize the process implemented in the previous work (Taguchi and Turki, 2020) to enable a comparative analysis of the results of the KTD based unsupervised FE with the previous results. The gene expression profiles was formatted as a tensor, $x_{ijkm} \in \mathbb{R}^{N \times 5 \times 2 \times 3}$, which indicated whether the gene expression of the ith gene of the jth cell line infected ($k = 1$) or not infected ($k = 2$, control) considering three biological replicates. The HOSVD was applied to x_{ijkm} to yield

$$x_{ijkm} = \sum_{\ell_1=1}^{5} \sum_{\ell_2=1}^{2} \sum_{\ell_3=1}^{m} \sum_{\ell_4=1}^{N} G(\ell_1 \ell_2 \ell_3 \ell_4) u_{\ell_1 j} u_{\ell_2 k} u_{\ell_3 m} u_{\ell_4 i} \tag{25}$$

bioRxiv preprint doi: https://doi.org/10.1101/2020.10.09.333195; this version posted October 12, 2020. The copyright holder for this preprint (which was not certified by peer review) is the author/funder. All rights reserved. No reuse allowed without permission.

where $G(\ell_1\ell_2\ell_3\ell_4) \in \mathbb{R}^{5\times2\times3\times N}$ is a core tensor, and $u_{\ell_1 j} \in \mathbb{R}^{5\times5}, u_{\ell_2 k} \in \mathbb{R}^{2\times2}, u_{\ell_3 m} \in \mathbb{R}^{3\times3}$ are orthogonal singular value matrices.

The purpose of the analysis was to identify the genes whose expression was distinct between the control and infected cells, independent of the cell lines and replicates. To this end, we selected ℓ_1, ℓ_2, ℓ_3 with constant $u_{\ell_1 j}$s and $u_{\ell_3 m}$s and $u_{\ell_2 1} = -u_{\ell_2 2}$. It was noted that $\ell_1 = \ell_3 = 1$ and $\ell_2 = 2$ could satisfy these requirements. Next, we identified $\ell_4 = 5$ associated with G having the largest absolute values given $\ell_1 = 1, \ell_2 = 2, \ell_3 = 1$. Once $\ell_4 = 5$ was selected, the P-values were assigned to gene i assuming the null hypothesis that $u_{\ell_4 i}$ obeys the Gaussian distribution:

$$P_i = P_{\chi^2}\left[> \left(\frac{u_{5i}}{\sigma_5}\right)^2\right] \tag{26}$$

where $P_{\chi^2}[> x]$ is the cumulative χ^2 distribution in which the argument is larger than x, and σ_5 is the standard deviation. The obtained P-values were corrected using the BH criterion. A total of 163 genes for which the adjusted P-values were less than 0.01 were selected and used to predict the drugs effective against COVID-19.

The objective of this study was to compare the performance of the KTD based unsupervised FE applied to x_{ijkm} with that of an existing study (Taguchi and Turki, 2020). Therefore, we employed the RBF kernel as

$$x_{jkmj'k'm'} = K(x_{ijkm}, x_{ij'k'm'}) = \exp\left\{-\alpha \sum_i \left(x_{ijkm} - x_{ij'k'm'}\right)^2\right\} \tag{27}$$

with $\alpha = 1 \times 10^{-6}$, to which the HOSVD was applied. We obtained

$$x_{jkmj'k'm'} = \sum_{\ell_1=1}^{5}\sum_{\ell_2=1}^{2}\sum_{\ell_3=1}^{3}\sum_{\ell'_1=1}^{5}\sum_{\ell'_2=1}^{2}\sum_{\ell'_3=1}^{3} G(\ell_1\ell_2\ell_3\ell'_1\ell'_2\ell'_3)u_{\ell_1 j}u_{\ell_2 k}u_{\ell_3 m}u_{\ell'_1 j'}u_{\ell'_2 k'}u_{\ell'_3 m'} \tag{28}$$

It was observed that u_{1j} and u_{1m} were constant, and $u_{\ell_2 1} = -u_{\ell_2 2}$ with $\ell_2 = 2$. We compared the $u_{1j}u_{2k}u_{1m}$ computed using the HOSVD and KTD with k. It was clarified that $u_{1j}u_{2k}u_{1m}$ computed using the KTD were more notably coincident with k (Fig. 3). Thus, the KTD exhibited a slight improvement over the HOSVD. Next, we were required

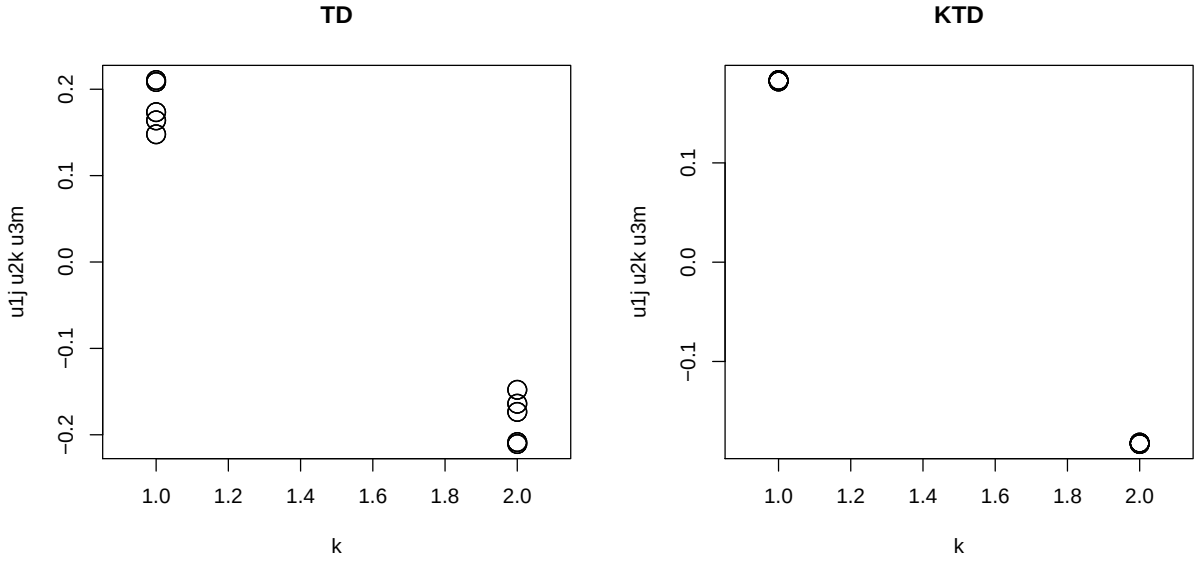

Figure 3: Scatter plot of $u_{1j}u_{2k}u_{1m}$ and k. left:TD, right:KTD.

to select genes, albeit the process was challenging as $u_{\ell_4 i}$ used for gene selection could not be obtained. To apply the

bioRxiv preprint doi: https://doi.org/10.1101/2020.10.09.333195; this version posted October 12, 2020. The copyright holder for this preprint (which was not certified by peer review) is the author/funder. All rights reserved. No reuse allowed without permission.

Table 2
Confusion matrix of the selected genes for the KTD and TD based unsupervised FE. In the KTD based unsupervised FE, the ranking was based on the correlation coefficients. The P-value computed using Fisher's exact test was $6.614619 \times 10^{-108}$, and the odds ratio was 168.

		KTD based unsupervised FE	
		rank > 163	rank ≤ 163
TD based	adjusted P-values ≥ 0.01	21540	94
unsupervised FE	adjusted P-values < 0.01	94	69

Table 3
Coincidence between 163 genes and human proteins that are known to interact with SARS-CoV-2 proteins during infection. The P-values were computed by applying Fisher's exact tests to the confusion matrix. For more details, please refer to the reference (Taguchi and Turki, 2020).

SARS-CoV-2 proteins	P values	Odds Ratio
SARS-CoV2 E	6.58×10^{-26}	9.84
SARS-CoV2 M	4.14×10^{-22}	7.26
SARS-CoV2 N	1.46×10^{-29}	13.63
SARS-CoV2 nsp1	5.51×10^{-15}	7.78
SARS-CoV2 nsp10	3.88×10^{-19}	11.02
SARS-CoV2 nsp11	1.2×10^{-27}	10.03
SARS-CoV2 nsp12	2.41×10^{-15}	7.72
SARS-CoV2 nsp13	7.41×10^{-28}	9.65
SARS-CoV2 nsp14	2.78×10^{-18}	10.18
SARS-CoV2 nsp15	1.08×10^{-14}	7.90
SARS-CoV2 nsp2	6.34×10^{-31}	11.11
SARS-CoV2 nsp4	5.53×10^{-26}	9.36
SARS-CoV2 nsp5	4.63×10^{-24}	11.91
SARS-CoV2 nsp5_C145A	4.65×10^{-14}	9.72
SARS-CoV2 nsp6	4.97×10^{-22}	7.94
SARS-CoV2 nsp7	1.61×10^{-22}	8.65
SARS-CoV2 nsp8	1.11×10^{-28}	9.84
SARS-CoV2 nsp9	6.71×10^{-28}	11.85
SARS-CoV2 orf10	1.16×10^{-26}	10.01
SARS-CoV2 orf3a	1.62×10^{-24}	8.80
SARS-CoV2 orf3b	2.50×10^{-27}	11.06
SARS-CoV2 orf6	8.03×10^{-22}	9.05
SARS-CoV2 orf7a	1.18×10^{-23}	8.57
SARS-CoV2 orf8	1.27×10^{-20}	7.25
SARS-CoV2 orf9b	9.11×10^{-28}	11.36
SARS-CoV2 orf9c	5.76×10^{-26}	7.69
SARS-CoV2 Spike	6.07×10^{-22}	8.81

KTD for gene selection, we recomputed $u_{1j}u_{2k}u_{1m}$ excluding i sequentially. In addition, the correlation coefficient between $u_{1j}u_{2k}u_{1m}$ and k were obtained. Subsequently, the is were ranked in ascending order of the absolute values of the correlation coefficients, as excluding the genes with expressions coincident with the distinction between $k = 1$ and $k = 2$ was expected to result in less significant (i.e., smaller absolute values of) correlation coefficients. Table 2 presents the confusion matrix of the selected genes. Notably, the genes are highly coincident and can even be regarded as identical considering that there existing twenty thousand genes, of which we selected only 163.

Next, we biologically evaluated the 163 genes selected using the KTD based unsupervised FE. In particular, we compared the selected 163 genes with gold standard human proteins that are known to interact with the SARS-CoV-2 proteins during infection (Gordon et al., 2020), following the procedure described in the previous study (Taguchi and Turki, 2020) (Table 3). Although the 163 genes selected by the KTD based unsupervised FE are highly coincident with the gold standard SARS-CoV-2 interacting human proteins, the results in Table 3 are slightly less coincident with the results for the gold standard SARS-CoV-2 interacting human proteins compared to the results presented in Table

bioRxiv preprint doi: https://doi.org/10.1101/2020.10.09.333195; this version posted October 12, 2020. The copyright holder for this preprint (which was not certified by peer review) is the author/funder. All rights reserved. No reuse allowed without permission.

S33 (Taguchi and Turki, 2020) corresponding to the application of the TD based unsupervised FE (Taguchi and Turki, 2020). Notably, only one protein group (SARS-CoV2 N) among the 27 protein groups in Table 3 exhibits a larger odds ratio in Table 3 (corresponding to the KTD based unsupervised FE) than that in Table S33 (corresponding to the TD based unsupervised FE (Taguchi and Turki, 2020)).

Tables 2 and 3 indicate two main findings. First, the KTD based unsupervised FE could not outperform the TD based unsupervised FE. At most, the results were comparable, similar to those when the KTD based unsupervised FE was applied to synthetic data simulating a *large p small n* problem (eq.(21)). It is thus likely that the KTD based unsupervised FE generally cannot outperform the TD based unsupervised FE when applied to *large p small n* problems. This aspect is likely why the TD based unsupervised FE can often outperform the state of art of methods despite its linearity. If linear methods such as the TD based unsupervised FE exhibit a performance that is comparable to that of non-linear methods such as the KTD based unsupervised FE, it is reasonable that the linear methods can outperform other more advanced methods since such methods are already competitive against non-linear methods. Second, although the KTD based unsupervised FE could not outperform the TD based unsupervised FE, the formulation of the KTD based unsupervised FE was effective. In other words, when this approach is applied to other problems, e.g., non *large p small n* problems, it is expected to outperform the TD based unsupervised FE, as in the case of the Swiss Roll (Fig. 2).

Kidney cancer data sets

In a previous work, we attempted to realize the integrated analysis of multiomics data by applying the TD based unsupervised FE (Ng and Taguchi, 2020). In the existing study (Ng and Taguchi, 2020), the objective was to select genes that act as prognostic biomarker for kidney cancer. To this end, the TD based unsupervised FE was employed to identify the differentially expressed genes (DEGs) between normal kidneys and tumors in two independent data sets. The TD based unsupervised FE successfully identified 72 mRNAs and 11 miRNAs for the first data set retrieved from the TCGA, and 209 mRNAs and 3 miRNAs for the second data set retrieved from the GEO. To extend this analysis, in the present study, the mRNA expression matrix $x_{ij} \in \mathbb{R}^{N\times M}$, which represents the ith mRNA expression in the jth sample, and the miRNA expression matrix $x_{kj} \in \mathbb{R}^{K\times M}$, which represents the kth miRNA expression in the jth sample were integrated into the tensor $x_{ijk} \in \mathbb{R}^{N\times M\times K}$ as

$$x_{ijk} = x_{ij}x_{kj} \tag{29}$$

and converted to a matrix $x_{ik} \in \mathbb{R}^{K\times M}$

$$x_{ik} = \sum_j x_{ijk} \tag{30}$$

to which the SVD was applied to yield

$$x_{ik} = \sum_\ell u_{\ell i}\lambda_\ell v_{\ell k}. \tag{31}$$

The missing singular value vectors attributed to the jth mRNA and miRNA samples were recovered as follows:

$$u^{\text{mRNA}}_{\ell j} = \sum_i x_{ij}u_{\ell i} \tag{32}$$

$$u^{\text{miRNA}}_{\ell j} = \sum_k x_{kj}u_{\ell k} \tag{33}$$

The P-values attributed to mRNAs and miRNAs were derived as

$$P_i = P_{\chi^2}\left[> \left(\frac{u_{2i}}{\sigma_2}\right)^2\right] \tag{34}$$

$$P_k = P_{\chi^2}\left[> \left(\frac{v_{2k}}{\sigma'_2}\right)^2\right] \tag{35}$$

as u^{mRNA}_{2j} and u^{miRNA}_{2j} were noted to be coincident with the distinction between the tumors and normal kidneys. The mRNAs and miRNAs with the adjusted P-values of less than 0.01 were selected.

bioRxiv preprint doi: https://doi.org/10.1101/2020.10.09.333195; this version posted October 12, 2020. The copyright holder for this preprint (which was not certified by peer review) is the author/funder. All rights reserved. No reuse allowed without permission.

Table 4
Performances of the linear and RBF kernel TD based unsupervised FE and that achieved in the previous study (Ng and Taguchi, 2020) by using Eq. (30). The P-values marked by an asterisk correspond to the most significant values.

1st data set (TCGA)	linear kernel	RBF kernel	previous study
u_{2j} (mRNA), tumor vs. normal kidney	6.78×10^{-45}*	1.06×10^{-44}	7.10 10-39
v_{2j} (miRNA), tumor vs. normal kidney	6.10×10^{-79}*	4.24×10^{-38}	2.13 10-71
u_{2j} vs. v_{2j} correlation coefficient	0.922 (7.18×10^{-135})	0.974 (5.93×10^{-212}*)	0.905 (1.63×10^{-121})
2nd data set (GEO)			
u_{2j} (mRNA), tumor vs. normal kidney	5.48×10^{-15}	5.42×10^{-15}	6.74×10^{-22}*
v_{2j} (miRNA), tumor vs. normal kidney	3.44×10^{-18}	1.17×10^{-13}	2.54×10^{-18}*
u_{2j} vs. v_{2j} correlation coefficient	0.954 (2.85×10^{-18})	0.966 (2.06×10^{-20}*)	0.931 (1.58×10^{-15})

Note that the kernel trick cannot be applied to this formulation as the summation is obtained over the sample index j and not the feature index i, k. Thus, instead, we formulated a kernel-trick-friendly integration of x_{ij} and x_{kj} as

$$x^{\text{mRNA}}_{jj'} = K(x_{ij}, x_{ij'}) = \sum_i x_{ij} x_{ij'} \tag{36}$$

$$x^{\text{miRNA}}_{jj'} = K(x_{kj}, x_{kj'}) = \sum_k x_{kj} x_{kj'} \tag{37}$$

$$x_{jj'} = \sum_{j''} x^{\text{mRNA}}_{jj''} x^{\text{miRNA}}_{j''j'} \tag{38}$$

to which the SVD can be applied to yield

$$x_{jj'} = \sum_\ell u_{\ell j} \lambda v_{\ell_{j'}}. \tag{39}$$

As this expression includes the inner product, for which the summation is obtained over the feature index i (eq. (36)) and k (eq. (37)), the expressions can be easily extended to the RBF kernel as

$$x^{\text{mRNA}}_{jj'} = K(x_{ij}, x_{ij'}) = \exp\left\{-\alpha \sum_i \left(x_{ij} - x_{ij'}\right)^2\right\} \tag{40}$$

$$x^{\text{miRNA}}_{jj'} = K(x_{kj}, x_{kj'}) = \exp\left\{-\alpha' \sum_k \left(x_{kj} - x_{kj'}\right)^2\right\}. \tag{41}$$

$x_{jj'}$ was computed using Eq. (38), and the SVD was applied to $x_{jj'}$, to obtain an expression similar to Eq. (39).

A possible biological validation of the performances of the KTD based unsupervised FE is by evaluating $u_{\ell j}$ and $v_{\ell j}$, corresponding to the mRNA and miRNA samples, respectively. Specifically, we consider whether

- $u_{\ell j}$s are distinct between tumorous and normal kidneys,
- $v_{\ell j}$s are distinct between tumorous and normal kidneys,
- $u_{\ell j}$s and $v_{\ell j}$s are coincident.

To examine the first point, we compute $u_{\ell j}$ and $v_{\ell j}$ using linear (eqs. (36) and (37)) and RBF (eqs. (40) and (41)) kernels ($\alpha = 10^{-12}$ and $\alpha' = 10^{-2}$). As in the previous study (Ng and Taguchi, 2020), the second singular value vectors, u_{2j} and v_{2j} are noted to be the most coincident with the aforementioned three requirements. Table 4 presents the comparisons of the P-values used to evaluate the aforementioned three conditions for the linear kernel, RBF kernel, and the approach employed in the previous study. The P-values to evaluate the distinction between tumorous and normal kidneys were computed through the t test, whereas those evaluating the coincidence between u_{2j} and v_{2j} were computed considering the correlation coefficients. Although the three types of approaches exhibited a reasonable performance, the RBF kernel that considered the non-linearity could not outperform the two other linear methods. The superiority of the RBF kernel was noted only when evaluating the coincidence. Thus, the non-linear method could not outperform the linear methods in the *large p small n* situation.

bioRxiv preprint doi: https://doi.org/10.1101/2020.10.09.333195; this version posted October 12, 2020. The copyright holder for this preprint (which was not certified by peer review) is the author/funder. All rights reserved. No reuse allowed without permission.

Table 5
Confusion matrix of the selected genes between the KTD (linear and RBF kernel) and TD based unsupervised FE (previous study (Ng and Taguchi, 2020) using Eq. (30)). The ranking in the KTD based unsupervised FE was t test based.

1st data set (TCGA)	linear kernel		RBF kernel	
mRNA	adjusted $P > 0.01$	adjusted $P < 0.01$	rank > 72	rank ≤ 72
previous study	19418	46	19437	27
	21	51	27	45
miRNA	adjusted $P > 0.01$	adjusted $P < 0.01$	rank > 11	rank ≤ 11
previous study	813	1	807	7
	10	1	7	4
2nd data set (GEO)	**linear kernel**		**RBF kernel**	
mRNA	adjusted $P > 0.01$	adjusted $P < 0.01$	rank > 209	rank ≤ 209
previous study	33764	25	33620	169
	61	148	169	40
miRNA	adjusted $P > 0.01$	adjusted $P < 0.01$	rank > 3	rank ≤ 3
previous study	316	0	315	1
	0	3	1	2

Finally, we compared the genes selected using the three methods. For the RBF, we followed the procedure pertaining to the RBF kernel TD based unsupervised FE applied to the SARS-CoV-2 infection cell lines. $x_{jj'}$ was computed excluding one of the miRNAs or mRNAs, and the SVD was applied to the obtained $x_{jj'}$ to obtain u_{2j}. The t test was applied to u_{2j} to compute the P-values using which the distinction of u_{2j} between tumorous and normal kidneys could be evaluated. When the first data set was considered, 72 top ranked mRNAs and 11 top ranked miRNAs having large (thus, less significant) P-values were selected, as the exclusion of the mRNAs or miRNAs distinct between the tumorous and normal kidneys was expected to decrease the significance of the distinct u_{2j} between the two entities. Similarly, when the second data set was considered, 209 top ranked mRNAs and 3 top ranked miRNAs were selected. For the linear kernel, the P-values attributed to the miRNAs and miRNAs were computed using Eqs. (34) and (35) with

$$u_{2i} = \sum_j x_{ij} u_{2j} \tag{42}$$

$$v_{2k} = \sum_j x_{kj} v_{2j}. \tag{43}$$

Subsequently, the mRNAs and miRNAs with adjusted P-values of less than 0.01 were selected. Table 5 presents the confusion matrices of the selected genes between the present study and previous study (Ng and Taguchi, 2020). The higher coincidence of the RBF or linear kernel with that obtained in the previous study depended on the data set. When the first and second data sets were considered, the RBF and linear kernels were more coincident with the findings of the previous study, respectively.

Although no gold standard data sets exist to evaluate the selected genes, one possible evaluation pertains to the coincidence of the selected genes between the first (TCGA) and second data sets (GEO). As these two data sets are independent, it is unlikely that commonly selected genes are present, and the selected genes are at most 1% of all genes. In the previous study (Ng and Taguchi, 2020) that employed Eq. (30), 11 genes were commonly selected between TCGA and GEO, whereas seven and eight genes were commonly selected between the TCGA and GEO for the linear and RBF kernels, respectively. Although these overlaps are still significant (using Fisher's exact test, $P = 3.43 \times 10^{-6}$, odds ratio: 12.54 for RBF kernel and $P = 1.27 \times 10^{-6}$, odds ratio: 11.59 for linear kernel), the values are inferior to those for the previous study (Ng and Taguchi, 2020) that involved 11 commonly selected genes ($P = 8.97 \times 10^{-11}$, odds ratio: 19.7). Thus, the KTD based unsupervised FEs are at most competitive with the TD based unsupervised FE in *large p small n* problems.

Discussion

In the aforementioned analyses, we successfully formalized the KTD based unsupervised FE to be applied to select DEGs. Although the implementation was effective, the KTD based unsupervised FE could not outperform the TD

bioRxiv preprint doi: https://doi.org/10.1101/2020.10.09.333195; this version posted October 12, 2020. The copyright holder for this preprint (which was not certified by peer review) is the author/funder. All rights reserved. No reuse allowed without permission.

based unsupervised FE that can address only the linearities. This finding may appear to be unexpected, as non-linear methods generally outperform linear methods pertaining to non-linear application by definition. Nevertheless, this expectation does not always hold, especially when the linear methods can achieve optimal solutions similar to those attained by non-linear methods.

As shown in Fig. 2(D), the KTD can precisely recognize the non-linearity in Swiss Rolls, at least partially. However, when the KTD based unsupervised FE is applied to *large p small n* problems, even the use of non-linear kernels could not outperform the TD based unsupervised FE or linear kernel based KTD based unsupervised FE. The reason for this aspect can be explained as follows. To represent complicated structures that only non-linear methods can recognize, many number of points are required. For example, to represent nth order polynomials, we need at least $n+1$ points. As the higher order polynomials can represent more complicated structures, more points are necessary to realize this representation. In *large p small n* problems, the number of samples in insufficient to represent complicated structures. As shown in Fig. 2, there exist 1,000 points in three-dimensional space. In contrast, in the considered *large p small n* problems, the number of samples ranges from a few tens to hundreds, whereas the number of corresponding features varies from 10^2 to 10^4. Thus, clearly, the points cannot effectively represent complicated structures. The TD based unsupervised FE, despite its linearity, has outperformed conventional statistical test based gene selection methods. It is rather unexpected that such a simple linear method can outperform more sophisticated advanced tools. Specifically, the TD based unsupervised FE has already achieved the performances that KTD based unsupervised FE employing non-linear kernels is expected to achieve in *large p small n* problems.

In addition, the KTD based unsupervised FE cannot exploit certain advantages that the TD based unsupervised FE exhibits. For example, as the KTD cannot yield singular value vectors attributed to the features (genes), we cannot apply the empirical P-value computation assuming that the singular value vectors obey the Gaussian distribution. Instead, we must repeatedly compute the singular value vectors excluding the features sequentially, which is a time-consuming process. In addition, the computation of inner products exponentially doubles the amount of memory required. As the number of samples is small, this aspect may not be an immediate problem. Nevertheless, this process for the first data set (TCGA) required half a day of CPU time while using 12 CPU units as the set included hundreds of samples. In contrast, the TD based unsupervised FE can complete the corresponding computation in a few minutes. Furthermore, the P-values computed by the KTD based unsupervised FE cannot be directly used for gene selection. When used to rank the genes, the process is effective (Tables 2 and 5). However, the process is ineffective when used to screen features directly, because the P-values are sufficiently small even after excluding one variable feature, e.g., those distinct between two classes (e.g., control and cancers). In this scenario, we cannot identify the number of features to be selected only considering the P-values. Nevertheless, this decision can be made using TD based unsupervised FE.

Despite these disadvantages of KTD based unsupervised FE, there may exist scenarios in which the results can be improved, whereas this aspect does not hold true for TD based unsupervised FE that lacks tunable parameters. At present, although we were unable to identify the cases in which the KTD unsupervised FE employing non-linear kernels could outperform the TD base unsupervised FE in *large p small n* problems, it is expected that the proposed approach can outperform the existing approach in scenarios involving *large p small n* problems in which the TD based unsupervised FE cannot achieve a high performance.

Methods

Data set

The data sets used in this study are all public domain. The information regarding the retrieval of these data sets has been presented in previous studies (Taguchi and Turki, 2020; Ng and Taguchi, 2020), in which the TD based unsupervised FE approach was applied to these data sets.

References

Gordon, D.E., Jang, G.M., Bouhaddou, M., Xu, J., Obernier, K., White, K.M., O'Meara, M.J., Rezelj, V.V., Guo, J.Z., Swaney, D.L., Tummino, T.A., Hüttenhain, R., Kaake, R.M., Richards, A.L., Tutuncuoglu, B., Foussard, H., Batra, J., Haas, K., Modak, M., Kim, M., Haas, P., Polacco, B.J., Braberg, H., Fabius, J.M., Eckhardt, M., Soucheray, M., Bennett, M.J., Cakir, M., McGregor, M.J., Li, Q., Meyer, B., Roesch, F., Vallet, T., Kain, A.M., Miorin, L., Moreno, E., Naing, Z.Z.C., Zhou, Y., Peng, S., Shi, Y., Zhang, Z., Shen, W., Kirby, I.T., Melnyk, J.E., Chorba, J.S., Lou, K., Dai, S.A., Barrio-Hernandez, I., Memon, D., Hernandez-Armenta, C., Lyu, J., Mathy, C.J.P., Perica, T., Pilla, K.B., Ganesan, S.J., Saltzberg, D.J., Rakesh, R., Liu, X., Rosenthal, S.B., Calviello, L., Venkataramanan, S., Liboy-Lugo, J., Lin, Y., Huang, X.P., Liu, Y., Wankowicz, S.A., Bohn, M., Safari, M., Ugur, F.S., Koh, C., Savar, N.S., Tran, Q.D., Shengjuler, D., Fletcher, S.J., O'Neal, M.C., Cai, Y., Chang, J.C.J.,

bioRxiv preprint doi: https://doi.org/10.1101/2020.10.09.333195; this version posted October 12, 2020. The copyright holder for this preprint (which was not certified by peer review) is the author/funder. All rights reserved. No reuse allowed without permission.

Broadhurst, D.J., Klippsten, S., Sharp, P.P., Wenzell, N.A., Kuzuoglu-Ozturk, D., Wang, H.Y., Trenker, R., Young, J.M., Cavero, D.A., Hiatt, J., Roth, T.L., Rathore, U., Subramanian, A., Noack, J., Hubert, M., Stroud, R.M., Frankel, A.D., Rosenberg, O.S., Verba, K.A., Agard, D.A., Ott, M., Emerman, M., Jura, N., von Zastrow, M., Verdin, E., Ashworth, A., Schwartz, O., d'Enfert, C., Mukherjee, S., Jacobson, M., Malik, H.S., Fujimori, D.G., Ideker, T., Craik, C.S., Floor, S.N., Fraser, J.S., Gross, J.D., Sali, A., Roth, B.L., Ruggero, D., Taunton, J., Kortemme, T., Beltrao, P., Vignuzzi, M., García-Sastre, A., Shokat, K.M., Shoichet, B.K., Krogan, N.J., 2020. A SARS-CoV-2 protein interaction map reveals targets for drug repurposing. Nature 583, 459–468. URL: https://doi.org/10.1038/s41586-020-2286-9, doi:10.1038/s41586-020-2286-9.

He, L., Lu, C.T., Ma, G., Wang, S., Shen, L., Yu, P.S., Ragin, A.B., 2017. Kernelized support tensor machines, in: Precup, D., Teh, Y.W. (Eds.), International Conference on Machine Learning, PMLR, International Convention Centre, Sydney, Australia. pp. 1442–1451. URL: http://proceedings.mlr.press/v70/he17a.html.

Liu, X., Guo, T., He, L., Yang, X., 2015. A low-rank approximation-based transductive support tensor machine for semisupervised classification. IEEE Transactions on Image Processing 24, 1825–1838.

Ng, K.L., Taguchi, Y.H., 2020. Identification of miRNA signatures for kidney renal clear cell carcinoma using the tensor-decomposition method. Scientific Reports 10. URL: https://doi.org/10.1038/s41598-020-71997-6, doi:10.1038/s41598-020-71997-6.

Schölkopf, B., 2000. The kernel trick for distances, in: Proceedings of the 13th International Conference on Neural Information Processing Systems, MIT Press, Cambridge, MA, USA. p. 283–289.

Signoretto, M., Lathauwer, L.D., Suykens, J.A., 2011. A kernel-based framework to tensorial data analysis. Neural Networks 24, 861–874. URL: https://doi.org/10.1016/j.neunet.2011.05.011, doi:10.1016/j.neunet.2011.05.011.

Signoretto, M., Olivetti, E., De Lathauwer, L., Suykens, J.A.K., 2012. Classification of multichannel signals with cumulant-based kernels. IEEE Transactions on Signal Processing 60, 2304–2314.

Taguchi, Y.H., 2020. Unsupervised Feature Extraction Applied to Bioinformatics. Springer International Publishing. URL: https://doi.org/10.1007/978-3-030-22456-1, doi:10.1007/978-3-030-22456-1.

Taguchi, Y.h., Turki, T., 2020. A new advanced in silico drug discovery method for novel coronavirus (sars-cov-2) with tensor decomposition-based unsupervised feature extraction. PLOS ONE 15, 1–16. URL: https://doi.org/10.1371/journal.pone.0238907, doi:10.1371/journal.pone.0238907.

Yan, S., Xu, D., Yang, Q., Zhang, L., Tang, X., Zhang, H., 2007. Multilinear discriminant analysis for face recognition. IEEE Transactions on Image Processing 16, 212–220.

Zhao, Q., Zhou, G., Adali, T., Zhang, L., Cichocki, A., 2013a. Kernelization of tensor-based models for multiway data analysis: Processing of multidimensional structured data. IEEE Signal Processing Magazine 30, 137–148.

Zhao, Q., Zhou, G., Adalı, T., Zhang, L., Cichocki, A., 2013b. Kernel-based tensor partial least squares for reconstruction of limb movements, in: 2013 IEEE International Conference on Acoustics, Speech and Signal Processing, pp. 3577–3581.

Acknowledgements (not compulsory)

This work was supported by KAKENHI [grant numbers 19H05270, 20H04848, and 20K12067] to YT and Deanship of Scientific Research (DSR) at King Abdulaziz University, Jeddah [grant number KEP-8-611-38] to TT.

Author contributions statement

YHT: Conceptualization, Formal analysis, Methodology, Software, Supervision, Writing – original draft, Writing – review & editing. TT: Data curation, Writing – original draft, Writing – review & editing

bioRxiv preprint doi: https://doi.org/10.1101/2020.10.09.333195; this version posted October 12, 2020. The copyright holder for this preprint (which was not certified by peer review) is the author/funder. All rights reserved. No reuse allowed without permission.

Y-H. Taguchi received a B.S. degree in physics from the Tokyo Institute of Technology and a Ph.D. degree in physics from the Tokyo Institute of Technology. He is currently a full professor with the Department of Physics, Chuo University, Japan. His works have been published in leading journals such as Physical Review Letters, Bioinformatics, and Scientific Reports. His research interests include bioinformatics, machine-learning, and non-linear physics. He is also an editorial board member of Frontiers in Genetics:RNA, PloS ONE, BMC Medical Genomics, Medicine (Lippincott Williams & Wilkins journal), BMC Research Notes, non-coding RNA (MDPI), and IPSJ Transaction on Bioinformatics.

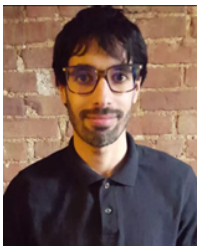

Turki Turki received a B.S. degree in computer science from King AbdulAziz University, an M.S. degree in computer science from NYU.POLY, and a Ph.D. degree in computer science from the New Jersey Institute of Technology. He is currently an assistant professor with the Department of Computer Science, King Abdulaziz University, Saudi Arabia. His research interests include Artificial Intelligence (Tensor Learning, Machine Learning, Deep Learning) and Bioinformatics. His research studies have been published in journals such as Expert Systems with Applications, Frontiers in Genetics, Current Pharmaceutical Design, Computers in Biology and Medicine, and Genes. Dr. Turki has served on the program committees of several international conferences and is currently a review editor for Frontiers in Artificial Intelligence and Frontiers in Big Data. In addition, he is an editorial board member of Computers in Biology and Medicine and Sustainable Computing: Informatics and Systems.